Thin Solid Films 519 (2011) 4421–4425

Contents lists available at ScienceDirect

Thin Solid Films

journal homepage: www.elsevier.com/locate/tsf

Boron doping: B/H/C/O gas-phase chemistry; H atom density dependences on pressure and wire temperature; puzzles regarding the gas-surface mechanism

Yuri A. Mankelevich [a,*], Michael N.R. Ashfold [b], Dane W. Comerford [b], Jie Ma [b], James C. Richley [b]

[a] Skobel'tsyn Institute of Nuclear Physics, Moscow State University, Moscow 119991, Russia
[b] School of Chemistry, University of Bristol, Bristol, BS8 1TS, UK

ARTICLE INFO

Available online 1 February 2011

Keywords:
Hot-filament CVD
Deposition process
Boron-doped diamond
Modeling

ABSTRACT

Experimental and modeling studies of the gas-phase chemistry occurring in dilute, hot filament (HF) activated $B_2H_6/CH_4/H_2$ gas mixtures appropriate for growth of boron-doped diamond are reported. The results of two-dimensional modeling of heat and mass transfer processes and the B/H/C chemistry prevailing in such HF activated gas mixtures (supplemented by reactions involving trace O_2 present as air impurity in the process gas mixture) are discussed and compared with measurements of B atom densities as functions of the hot wire temperature T_w and distance from the wire. Most of the B_2H_6 molecules that diffuse from the cool, near-wall regions into the hot, near wire region are thermally decomposed (yielding two BH_3 molecules as primary products) and then converted into various 'active' B-containing species like B, BH and BH_2 — some of which are able to accommodate into the growing diamond film. H-shifting reactions $BH_x + H \leftrightarrow BH_{x-1} + H_2$ enable rapid inter-conversion between the various BH_x ($x=0$–3) species and the BH_x source is limited by diffusional transfer of B_2H_6. H atoms play several key roles — *e.g.* activating the process gas mixture, and driving inter-conversions between the various $H_xB_yC_zO_{z'}$ species. We show that the T_w and gas pressure dependences of the H atom production rate (by H_2 dissociation on the HF surface) can be accommodated by a simple gas-surface reaction model.

© 2011 Elsevier B.V. All rights reserved.

1. Introduction

Hot-filament (HF) activation of dilute hydrocarbon/H_2 (*e.g.* CH_4/H_2) gas mixtures is an established low-cost route for diamond chemical vapour deposition (CVD) [1–3]. Addition of trace amounts of a boron containing precursor (*e.g.* 10–1000 ppm of B_2H_6) during diamond CVD is of considerable interest, as incorporated B atoms act as acceptors (E_a~0.37 eV) and impart p-type semiconductivity to the as-grown B-doped diamond [4]. B-doped diamond is attracting interest for its potential application in electronic and optical devices [5,6], bio-sensing [7], and as a result of its more recently discovered superconductivity [8,9]. All such applications require reliable recipes for forming high quality B-doped diamond, with controllable doping levels; hence the emerging need for a much fuller understanding of the doping processes and of the B/H/C chemistry. However, the details of the gas-phase and gas-surface chemistry involved in the growth of B-doped CVD diamond are still poorly understood. The literature contains only a handful of papers reporting diagnostics relevant to B-containing microwave (MW) plasmas, though several studies have sought to establish relationships between diamond film quality, dopant concentration and reactor parameters such as the B_2H_6 flow rate (or the input [B]/[C] ratio), substrate temperature, *etc.* [10–12]. We have embarked on combined experimental and theoretical studies of the B/H/C chemistry prevailing in both HFCVD [13] and MW plasma enhanced (PE) CVD reactors [14,15]. The experimental part of the HFCVD project has involved use of resonance enhanced multiphoton ionization (REMPI) techniques to measure spatially resolved relative number densities of B (and H) atoms – henceforth represented as [B], [H], *etc.* – as functions of process conditions (*e.g.* the hot wire material, and its temperature T_w, gas pressure p, the B_2H_6/H_2 mixing ratio, and the presence (or not) of added CH_4) [13]. The complementary modeling builds on previous analyses of CH_4/H_2 [3,16–18], $CH_4/NH_3/H_2$ [19], B_2H_6/H_2 and $CH_4/B_2H_6/H_2$ [13] gas-phase and gas-surface chemistry in HFCVD reactors. One of the challenges of the present study is to determine the important reaction pathways (with known and/or assumed rate coefficients) in B/C/H gas mixtures under typical HFCVD reactor conditions. Our recent studies of B/H/C chemistry in a MW PECVD reactor [14,15] showed that trace amounts of O_2 impurity (air leakage, impurity in source gas) present at concentrations comparable to the B_2H_6 concentrations typically used in B-doped diamond CVD can have a major effect on the BH_x concentrations — hence the need to establish the much more complex, four component, B/H/C/O chemical mechanism.

2. Modeling of HFCVD reactor processes in B/H/C/O mixtures

To start the study of B/H/C/(O) chemistry in HFCVD reactors one first needs to be able to describe the processes involved in diamond

* Corresponding author. Tel.: +7 495 9394102.
E-mail address: ymankelevich@mics.msu.su (Y.A. Mankelevich).

0040-6090/$ – see front matter © 2011 Elsevier B.V. All rights reserved.
doi:10.1016/j.tsf.2011.01.328

deposition from conventional (*e.g.* 1%CH_4/H_2) mixtures, *i.e.* proper treatments of the catalytic dissociation of H_2 on the HF surface, the H/C gas-phase chemistry, the gas temperature (T_{gas}) and species concentration distributions, diamond growth models, *etc*. Then one needs to collect and analyze scarce data on B/H/O chemical kinetics and thermochemistry from previous studies under conditions that, as a rule, are far from the typical HFCVD conditions. These include combustion studies of boranes (B_xH_y) in the search for high-energy fuels [20–22], studies of MW PECVD reactors [14,15,23,24], theoretical studies of various B_xH_y, $B_xH_yO_z$ species, their structures and reactions with H, H_2, H_xO_y and C_xH_y species [20–22,25,26], and B_2H_6 dissociation studies (in B_2H_6 and B_2H_6/H_2 mixtures) [27]. Below we describe the main stages of our model development.

2.1. Catalytic H_2 dissociation on HF surface

H atoms play a crucial role in activating the process gas mixtures and initiating the various inter-conversions within and between the CH_x and C_2H_y families (and $H_xB_yC_zO_{z'}$ species in B/H/C/O mixtures). Previous theoretical [16,18,28,29] and experimental studies have explored H atom densities (as functions of process parameters) by, for example, REMPI [3,13], laser induced fluorescence [30], third-harmonic generation [31], and calorimetric studies of the filament power balance in order to establish the fractions of supplied electrical power expended through radiation, conduction and catalytic H_2 dissociation [18,32,33]. Such studies have shown that the distribution of H atom densities under typical HFCVD reactor conditions (*e.g.* p ~ 10–50 Torr, T_w ~ 2300–2700 K) is largely established by the balance of production (H_2 catalytic dissociation on the HF surface), loss (both recombination on the cold reactor walls, substrate, substrate holder, and consumption in gas-phase reactions) and diffusional transfer. The H atom source term should be well described as a function of process parameters like p and T_w, but various aspects of the dissociation mechanism and measured dependences remain unclear. For example, the input powers required to maintain the hot wire at a given T_w appear to saturate at $p(H_2)$ ~ 10–20 Torr, as do the measured H atom concentrations (which thereafter remain flat or even decline slightly upon increasing p ~ 100 Torr) — in marked contradiction with expectations based on the ~5-fold increase of the number of collisions between H_2 molecules and the HF surface and the ~5-fold decrease in the diffusional coefficient (D ~ $1/p$) [18]. In addition, T_w dependent measurements of the effective enthalpy for forming H atoms return a value, ΔH ~ 2.45 eV, that is much lower than the H_2 bond strength [18]. In an attempt to explain such apparent paradoxes, we recently proposed a self-consistent approach based on analytical distributions of T_{gas} and H atom concentrations in the immediate proximity of the HF, and a simple gas-surface model based on two effective (and reversible) chemisorption/desorption reactions:

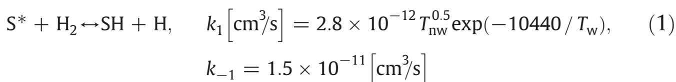

$$S^* + H_2 \leftrightarrow SH + H, \quad k_1\left[\mathrm{cm^3/s}\right] = 2.8\times10^{-12}T_{nw}^{0.5}\exp(-10440/T_w), \quad k_{-1} = 1.5\times10^{-11}\left[\mathrm{cm^3/s}\right] \tag{1}$$

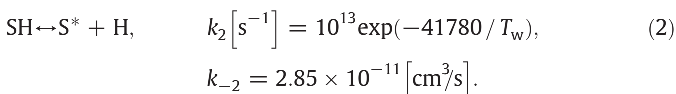

$$SH \leftrightarrow S^* + H, \quad k_2\left[\mathrm{s^{-1}}\right] = 10^{13}\exp(-41780/T_w), \quad k_{-2} = 2.85\times10^{-11}\left[\mathrm{cm^3/s}\right]. \tag{2}$$

S^* and SH are the active (free) and H-terminated sites on the HF surface, respectively, $[S_0]=[SH]+[S^*]$ is the total surface site density per unit area, $T_{nw}=T_{gas}(d=0)$ is the gas temperature adjacent to the hot wire surface, d is the distance from the HF, and k_i are the rate coefficients adopted in [18] for a bare Ta wire. This approach affords a consistent description of all of the experimental observations, and the measured trends upon varying p and T_w. In particular, the saturation of the catalytic source term Q [$cm^{-2}\,s^{-1}$] (where Q is the number of H atoms produced per second per unit area of hot surface, *i.e.* $Q=2(R_1-R_{-1})=2(R_2-R_{-2})$ in terms of reaction rates R_i ($i=1, 2$) [18]) and of the H atom densities measured a few mm from the HF surface are explained by the appropriate drop of the free site fraction $[S^*]/[S_0]$ — as can be seen in Fig. 1, which illustrates results from [18] for the case of a bare Ta wire at $T_w=2440$ K in H_2 gas. This plot also highlights the sensitivity of the $[H](d=2\text{ mm})/[H](d=0)$ ratio to $p(H_2)$: the observed saturation of the H atom density measured a few mm from the HF surface does not imply a similar saturation for the H atom concentration at $d=0$. This effect, which is induced by the very steep gradients in T_{gas} and [H] near the HF [18] and the decline in the diffusion coefficient with p (D_H ~ $1/p$), illustrates a limitation of using H atom concentrations measured near the HF as a proxy for the H atom densities at the HF surface itself when varying $p(H_2)$: such an assumption introduces a >200% error in the $[H](d=2\text{ mm})/[H](d=0)$ ratio across the range $20<p(H_2)<100$ Torr. The catalytic source term Q is an important parameter for the 2D/3D models discussed below.

2.2. 2D/3D models of HFCVD reactor processes

Another important element in our theoretical studies is the development of 2D(r,z) and 3D(x,y,z) models to describe (i) activation of the reactive mixture (*e.g.* gas heating, catalytic H atom production on the HF and, in the present case, loss of gas-phase boron by incorporation at the HF surface), (ii) gas-phase processes (heat and mass transfer, and chemical kinetics), and (iii) gas-surface processes at the substrate. The models involve the conservation equations for mass, momentum, energy, and species concentrations, together with appropriate initial and boundary conditions, thermal and caloric equations of state. These equations are integrated numerically to yield spatial distributions of T_{gas} and, in the case of H/C gas mixtures, the various H_xC_y species (H, H_2, CH_x ($x=0$–4), C_2H_y($y=0$–6)) densities. The calculated results for different reactor parameters succeed in reproducing a wealth of data and trends observed experimentally [3,16–19]. For the present study of B-doped diamond deposition, the chemical mechanism was necessarily expanded to incorporate the B/H/C/O mechanism described below.

Most of the calculations in the present study employed the computationally less time consuming 2D(r,z) model and base conditions as follows: $p=20$ Torr, substrate temperature $T_{sub}=1073$ K, flow rates $F(CH_4)=1$ standard cm^3 per minute (sccm), $F(H_2)=99$ sccm, $F(B_2H_6)=0.0475$ sccm, and T_w values of 2073, 2300 and 2573 K. The reactor is represented in cylindrical coordinates, with z parallel to the direction of gas flow. The modeling considers a part of the Bristol HFCVD reactor (a chamber based on a six-way cross). The model reactor volume was bounded in the radial and vertical directions by, respectively, $0<r<25$ mm and -10 mm$<z<30$ mm, with the point (0,0) defining

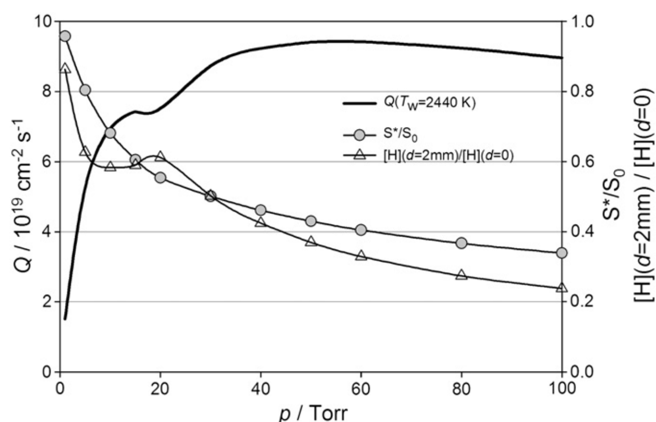

Fig. 1. Plot illustrating the calculated $p(H_2)$ dependences of the catalytic H atom production rate Q, the free site fraction $[S^*]/[S_0]$ and the $[H](d=2\text{ mm})/[H](d=0)$ ratio for a bare Ta HW at $T_w=2440$ K.

the center of the substrate. The assumed cylindrical symmetry offers, at best, an approximate representation of the location and volume of the experimental Ta (Re) HF (0.250 mm diameter, 7 turns with coil diameter ~3 mm and coil length ~8 mm, providing a geometrical hot surface area S_{hot}~0.57 cm^2). In the model, the HF volume was confined within the cylinder $r<2$ mm, $10<z<13$ mm. The temperature drop $\Delta T = T_w - T_{gas}(d=0)$ ~250 K between the HF surface and the immediate gas phase was estimated using the Smoluchowski formula and an H_2 accommodation coefficient ~0.3–0.4 [34]. Estimates for the catalytic H atom production rates $Q(T_w)$ per cm^2 of the HF surface were taken from previous data [13,18,19], yielding the effective enthalpy ΔH~2.18 eV for borodized Ta (*i.e.* TaB) wires at $T_w<2400$ K and the decline of H atom concentration at $T_w>2400$ K [35]. H atom production rates $Q(T_w$,TaB) ~9×10^{18}, 3×10^{19} and 4.85×10^{19} cm^{-2} s^{-1} were used here for borodized Ta wires at $T_w=2073$, 2300 and 2573 K, respectively, and $Q(T_w$,TaCB$)=Q(T_w$,TaB)/2 for carburized-borodized Ta wires in B/H/C mixtures. The substrate and substrate holder located at ($r<1$ mm, $-10<z<0$ mm) in the present modeling was chosen to have minimal radius (*i.e.* 1 mm, which is the grid cell size in both the r and z directions) simply to retain the possibility of calculating species densities just above the substrate surface ($r<1$ mm, $z=0$) and thus to compare with the B atom profiles measured experimentally in the absence of any substrate and substrate holder. The regions ($r<3$ mm, $z=30$ mm) and ($23<r<25$ mm, $z=-10$ mm) define the gas inlet and outlet positions in the model, T_{sub} was kept constant (at 1073 K) and T_{gas} at the reactor walls was set to 300 K.

2.3. B/H/C/O chemical mechanism

The available chemical and thermochemical data for B-containing species together with our recent thorough experimental and theoretical study of MW activated B_2H_6/Ar/H_2 [14] and B_2H_6/CH_4/Ar/H_2 [15] plasmas used for CVD of B-doped diamond have allowed development of a B/H/C/O chemical mechanism and its testing on a variety of experimental measurements [14,15]. Briefly, the absolute column densities of ground state B atoms, electronically excited H($n=2$) atoms, and BH, CH and C_2 radicals in MW activated B/H/C/Ar plasmas have been determined by cavity ring down spectroscopy, as functions of process conditions. Optical emission spectroscopy has also been used to explore variations in the relative densities of electronically excited H atoms, H_2 molecules and BH, CH and C_2 radicals. These experimental data have been complemented by extensive 2D(r,z) modeling of the plasma chemistry, and have enabled substantial refinements to the existing B/H/C/O thermochemistry and chemical kinetics. The combined experimental/2D modeling study indicates that deposition of B-containing material on the reactor walls (mainly from B atom adsorption, with some participation from H_2O) becomes progressively less important at higher $F(CH_4)$ [15]. B/H/C/(O) coupling reactions are deduced to play important (but still incompletely understood) roles in determining the local BH_x ($x=0$–3) number densities. Most (75–80%) of the B_2H_6 in the input gas mixture is efficiently dissociated in the hot plasma and near plasma regions, at gas temperatures $T_{gas}>1000$ K [15]. The resulting BH_x species undergo further processing, and much of the boron is deduced to be stored as more stable $H_xB_yC_zO_{z'}$ reservoir species like HBO, H_2BO, H_3COBH_2 and, particularly, CH_2CHBH_2 and $CH_3CH_2BH_2$. The spatial profiles of the various BH_x species reflect the complex balance of diffusional transfer and inter-conversions between the various families of B-containing species in the different local environments (T_{gas}, [H], [H_2O], [C_xH_y], *etc.*). Key conversions in the mechanism proposed here include $BH_x \leftrightarrow H_yBC_z$ (involving C_2H_2 and C_2H_4) and $BH_x \rightarrow H_yBO \rightarrow H_zCOBH_y \rightarrow BH_x$ (via reactions with, or activation by, H_2O, CH_x species and/or H atoms).

These refined B/H/C and B/H/C/O mechanisms were embedded in the existing 2D(r,z) and 3D(x,y,z) models of a HFCVD reactor to determine the important reaction pathways under typical HFCVD reactor conditions. The B/H/C chemical kinetics mechanism employed includes 112 direct and reverse reactions for 23 species (H, H_2, CH_x ($x=0$–4), C_2H_y($y=0$–6), BH_x($x=0$–3), B_2H_6, CH_2CHBH_2 and $CH_3CH_2BH_2$). As mentioned above, trace amounts of O_2 impurity (from air leakage, and/or as an impurity in the source gas) at number densities comparable to the typical B_2H_6 concentrations can have a serious impact on the BH_x species concentrations. To trace such effects of oxygen, additional conversions involving HBO, H_2BO, O_2, O, OH, H_2O, CO, H_xCO, H_xCCO, $x=1,2$, and H_xCOBH_2 ($x\leq3$) species have been introduced in the full B/H/C/O chemical mechanism, which includes 276 direct and reverse reactions.

3. Calculated results: B/H/C/(O) chemistry in HFCVD reactor conditions

All aspects of the deceptively simple HFCVD reactor processes described above were incorporated in the 2D(r,z) model for simulating the B-doped diamond deposition process. Armed with such a model, we can predict spatial distributions of hydrogen, hydrocarbon and B-containing species in the Bristol HFCVD reactor, for comparison with measured B atom profiles and their dependence on T_w, distance d from the HF and CH_4 fractions (0 or 1%). The observation that [B] doubles when $F(CH_4)$ was reduced to zero forced us to introduce an additional diborane dissociation channel involving

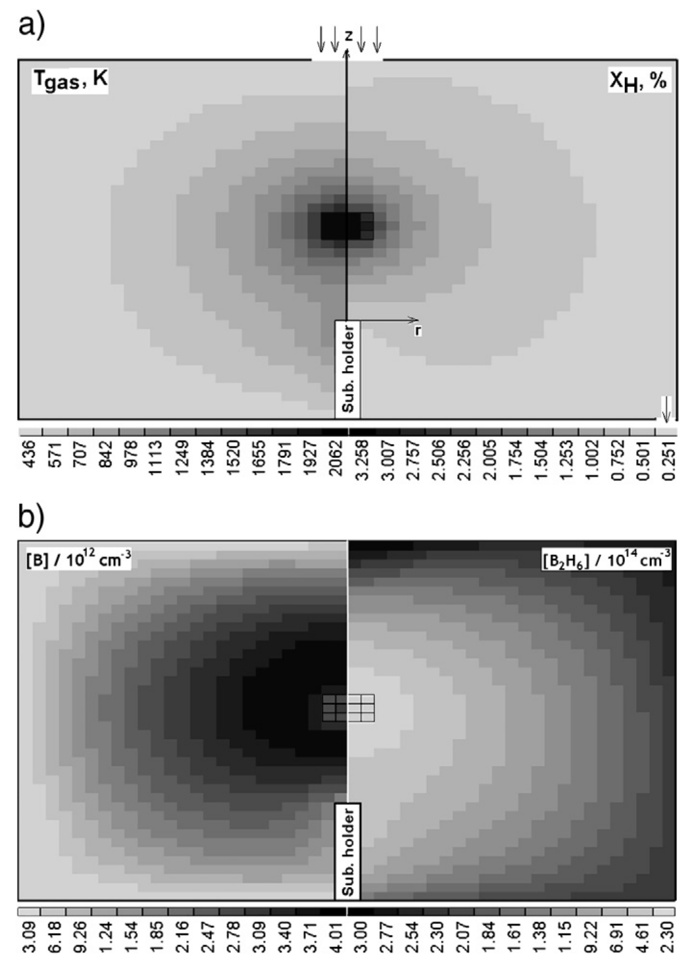

Fig. 2. Calculated 2D(r,z) distributions of a) the T_{gas} (left half-panel) and the H atom mole fraction X_H, and b) the B atom (left half-panel) and B_2H_6 concentrations for 0.0475%B_2H_6/1%CH_4/H_2 mixture, $T_w=2300$ K and $p=20$ Torr. The substrate holder and the HW volume (rectangular mesh at the image center) assumed in the modeling are indicated also. The model reactor volume was bounded in the radial and vertical directions by, respectively, $0<r<25$ mm and -10 mm$<z<30$ mm, the point (0,0) is the center of the substrate.

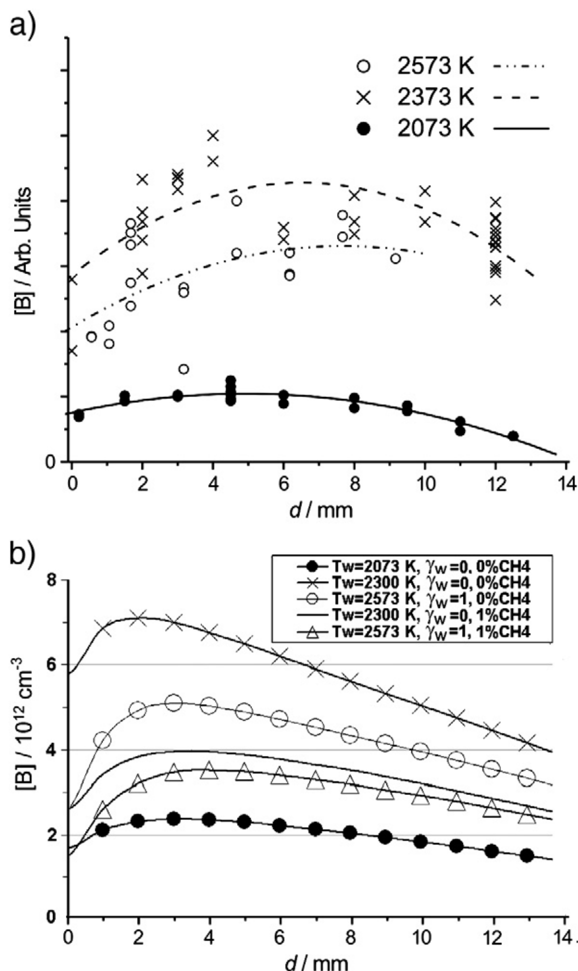

Fig. 3. a) Plots of [B] vs d using a borodized Ta HW, measured in $0.0475\%B_2H_6/H_2$ mixture at the specified T_w values. The superposed lines through the data are intended merely to guide the eye. b) Plots of calculated [B] vs d for $0.0475\%B_2H_6/x\%CH_4/H_2$ ($x=0$ or 1) mixtures and $T_w=2073$, 2300 and 2573 K assuming B atom loss probability on the wire surface $\gamma_W=0$ or $\gamma_W=1$ (for $T_w=2573$ K).

reaction with H atoms, *i.e.* $B_2H_6+H\rightarrow BH_4+BH_3\rightarrow 2BH_3+H$. The total B_2H_6 decomposition rate was thus described as follows,

$$B_2H_6+M\rightarrow BH_3+BH_3+M,\quad k\left[\mathrm{cm^3\,s^{-1}}\right]=4.2\times10^{-7}\exp\left(-17008/T_{gas}\right) \quad (3)$$

with $M=B_2H_6$ (enhancement factor = 1), C_2H_2 (0.1), CH_4 (0.1), H (0.05). Test calculations assuming various different probabilities, $\gamma_{B_2H_6}$, for the catalysed decomposition of B_2H_6 on the HF surface indicate that this process might make a contribution to BH_3 production comparable to that from thermal dissociation only at low T_w and high $\gamma_{B_2H_6}$ (*e.g.* surface catalysed dissociation might contribute ~50% of the total BH_3 production rate at $T_w=2073$ K and $\gamma_{B_2H_6}=0.5$).

The results of the 2D modeling in the $0.0475\%B_2H_6/1\%CH_4/H_2$ mixture are illustrated by the 2D(r,z) distributions of T_{gas}, the H atom mole fraction, and the B atom and B_2H_6 number densities shown in Fig. 2a and b, respectively, for $T_w=2300$ K. Most of the B_2H_6 molecules that diffuse from the cool, near-wall regions into the hot, near HF region are thermally decomposed, giving two BH_3 molecules as primary products, which are then further converted into 'active' B-containing species like B, BH and BH_2 — some of which are able to accommodate into the growing diamond film and at the reactor walls. The H-shifting reactions $BH_x+H\leftrightarrow BH_{x-1}+H_2$ enable rapid inter-conversion between the various BH_x ($x=0$–3) species, favoring B atoms in the wire–substrate gap; the BH_x source is seen to be limited by diffusional transfer of B_2H_6. The calculations show that B atom loss at the reactor walls affects both the absolute concentrations of the various BH_x species, and their profiles.

Comparison between Fig. 3a and b shows that the modeling reproduces the B atom spatial profiles observed with the 0.0475% B_2H_6/H_2 mixture well if we assume a probability of B atom loss at the wall, $\gamma_{wall}=0.1$ [13]. The general decline in [B] at large d can be reproduced with smaller γ_{wall} values also, but all calculations with $\gamma_{wall}=0$ return [B] profiles which increase with increasing d. The modeling fails to replicate the observed fall in [B] at $T_w>2350$ K but, as previously [13], the measured fall can be reproduced reasonably well by assuming a marked increase in the loss probability γ_w of B atoms at the HF surface at temperatures that exceed the melting temperatures of boron (T_{mp}~2350 K) and TaB (T_{mp}~2313 K). As an illustration of this effect, Fig. 3b shows the B atom concentration at $T_w=2573$ K calculated assuming $\gamma_w=1$. The last two curves in Fig. 3b, for the case of a 0.0475% $B_2H_6/1\%CH_4/H_2$ mixture with $T_w=2300$ K, $\gamma_w=0$ and $T_w=2573$ K, $\gamma_w=1$, respectively, successfully mimic the experimentally observed [13] fall in [B] at $d=3$ mm upon introducing $F(CH_4)=1$ sccm.

Preliminary calculations exploring the effect of O_2 impurity (at concentrations of 100 ppm, much less than the 500 ppm of B_2H_6 assumed in our base conditions) show conversion of BH_x species to H_yBO($y=1$,2) species (mainly through the reaction of B atoms with H_2O), but the B atom densities are only reduced seriously once $F(O_2)$ approaches $F(B_2H_6)$. Thus, we here focus on presenting the calculated species distributions above the substrate surface for the specific cases of a $0.01\%B_2H_6/0.01\%O_2/1\%CH_4/H_2$ mixture (*i.e.* $F(B_2H_6)=F(O_2)$) at $T_w=2300$ K and an O_2-free $0.0475\%B_2H_6/1\%CH_4/H_2$ mixture at T_w values of 2300 and 2573 K. Table 1 shows the calculated species concentrations at $r=0$, $z=0.5$ mm for these three sets of conditions. Inspection of these data clearly illustrates the reduction in [B] induced by the presence of O_2 (*i.e.* [B](column 1) < [B](column 2)/4.75 (because [B]~$F(B_2H_6)$ for the O_2-free case). Given these densities, we can also estimate the diamond growth rate G which, under these conditions, will

Table 1
Species concentrations [cm^{-3}] above the substrate (at $r=0$, $z=0.5$ mm) for $0.01\%B_2H_6/0.01\%O_2/1\%CH_4/H_2$ mixture ($T_w=2300$ K, $\gamma_W=0$) and $0.0475\%B_2H_6/1\%CH_4/H_2$ mixtures $T_w=2300$ ($\gamma_W=0$) and 2573 K ($\gamma_W=1$). The number format 6.05E+14 stands for 6.05×10^{14}. The last row shows the estimated diamond growth rate, G, in μm/h.

T_w/K	2300	2300	2573
H	6.03E+14	6.05E+14	7.93E+14
CH_3	1.49E+13	1.49E+13	2.45E+13
C_2H_2	6.54E+12	5.40E+12	1.72E+13
CH_2	4.73E+09	4.75E+09	1.26E+10
CH_2(S)	8.23E+07	8.27E+07	2.17E+08
CH	1.02E+08	1.02E+08	3.52E+08
C	3.18E+08	3.21E+08	1.92E+09
C_2(a)	3.00E+07	2.99E+07	2.32E+08
C_2(X)	5.28E+04	5.27E+04	4.64E+05
C_2H	1.70E+05	1.44E+05	9.19E+05
C_2H_6	1.90E+12	2.01E+12	2.34E+12
C_2H_4	1.64E+12	1.58E+12	3.10E+12
C_2H_5	8.12E+09	8.50E+09	1.19E+10
C_2H_3	1.36E+10	1.18E+10	3.38E+10
B_2H_6	5.59E+12	2.69E+13	2.09E+13
BH_3	8.88E+10	3.45E+11	1.52E+11
BH_2	3.86E+08	1.50E+09	9.18E+08
BH	5.78E+08	4.60E+09	4.54E+09
B	1.07E+11	1.73E+12	1.76E+12
$CHCH_2BH_2$	2.96E+11	8.06E+11	7.92E+11
$CH_2CH_3BH_2$	6.08E+10	2.39E+11	1.61E+11
CH_4	9.41E+14	9.41E+14	8.92E+14
H_2	1.97E+17	1.97E+17	1.93E+17
H_xBO	4.08E+12		
O_2	2.22E+12		
H_2O	3.99E+12		
CO	9.55E+11		
2 $F(B_2H_6)/F(CH_4)$	0.02	0.1	0.1
[B]/[CH_3]	0.007	0.12	0.07
G, μm/h	0.16	0.16	0.26

be dictated by the incident density of CH_3 radicals. The growth rate was estimated from the formula [36,37]

$$G = 0.075 \times 3.8 \times 10^{-14} T_{sub}^{0.5}[CH_3] / \{1 + 0.3 \cdot \exp(3430 / T_{sub}) + 0.1 \cdot \exp(-4420 / T_{sub})[H_2] / [H]\}. \quad (4)$$

The predicted [B]/[CH_3] number density ratio at a growing diamond surface (~0.07–0.12) is close to $2\,F(B_2H_6)/F(CH_4) \approx 0.1$ for the O_2-free cases. For a reliable estimation of the likely B incorporation rate a more detailed simulation employing the full-scale HFCVD reactor geometry and experimental characterization of B-doping level would be required. At this stage, the present modeling only allows us to conclude that B-doping of CVD diamond in HFCVD reactors is likely to be provided by B atoms, which are the dominant BH_x species near the substrate and the HF.

Acknowledgements

The Bristol–Moscow collaboration is supported by a Royal Society Joint Project Grant. YuAM acknowledges support from RF Government for Key Science Schools grant No. 3322.2010.2.

References

[1] F.G. Celii, J.E. Butler, Ann. Rev. Phys. Chem. 42 (1991) 643.
[2] D.G. Goodwin, J.E. Butler, in: M.A. Prelas, G. Popovici, L.G. Bigelow (Eds.), Handbook of Industrial Diamonds and Diam. Films, M. Dekker, New York, 1998, p. 527.
[3] M.N.R. Ashfold, P.W. May, J.R. Petherbridge, K.N. Rosser, J.A. Smith, Yu.A. Mankelevich, N.V. Suetin, Phys. Chem. Chem. Phys. 3 (2001) 3471.
[4] A. Deneuville, Semicond. Semimet. 76 (2003) 183, and references therein.
[5] E. Kohn, A. Denisenko, in: R.S. Sussmann (Ed.), CVD Diamond for Electronic Devices and Sensors, John Wiley and Sons, 2009,, Chap. 14.
[6] S. Koizumi, K. Watanabe, F. Hasegawa, H. Kanda, Science 292 (2001) 1899.
[7] C.E. Nebel, B. Rezek, D. Shin, H. Uetsuka, N. Yang, J. Phys. D Appl. Phys. 40 (2007) 6443.
[8] E.A. Ekimov, V.A. Sidorov, E.D. Bauer, N.N. Mel'nik, N.J. Curro, J.D. Thompson, S.M. Stishov, Nature 428 (2004) 542.
[9] Y. Takano, M. Nagao, I. Sakaguchi, M. Tachiki, T. Hatano, K. Kobayashi, H. Umezawa, H. Kawarada, Appl. Phys. Lett. 85 (2004) 2851.
[10] E. Gheeraert, A. Deneuville, J. Mambou, Carbon 37 (1999) 107.
[11] B.J. Lee, B.T. Ahn, Y.J. Baik, Diamond Relat. Mater. 8 (1999) 251.
[12] R. Ramamurti, M. Becker, T. Schuelke, T. Grotjohn, D. Reinhard, J. Asmussen, Diamond Relat. Mater. 17 (2008) 1320.
[13] D.W. Comerford, A. Cheesman, T.P.F. Carpenter, D.M.E. Davies, N.A. Fox, R.S. Sage, J.A. Smith, M.N.R. Ashfold, Y.A. Mankelevich, J. Phys. Chem. A 110 (2006) 2868.
[14] J. Ma, J.C. Richley, D.R.W. Davies, A. Cheesman, M.N.R. Ashfold, Y.A. Mankelevich, J. Phys. Chem. A 114 (2010) 2447.
[15] J. Ma, J.C. Richley, D.R.W. Davies, M.N.R. Ashfold, Y.A. Mankelevich, J. Phys. Chem. A 114 (2010) 10076.
[16] Y.A. Mankelevich, A.T. Rakhimov, N.V. Suetin, Diamond Relat. Mater. 5 (1996) 888.
[17] Y.A. Mankelevich, A.T. Rakhimov, N.V. Suetin, Diamond Relat. Mater. 7 (1998) 1133.
[18] D.W. Comerford, J.A. Smith, M.N.R. Ashfold, Y.A. Mankelevich, J. Chem. Phys. 131 (2009) 044326.
[19] J.A. Smith, J.B. Wills, H.S. Moores, A.J. Orr-Ewing, M.N.R. Ashfold, Yu.A. Mankelevich, N.V. Suetin, J. Appl. Phys. 92 (2002) 672.
[20] R.A. Yetter, H. Rabitz, F.L. Dryer, R.C. Brown, C.E. Kolb, Combust. Flame 83 (1991) 43.
[21] L. Pasternack, Combust. Flame 90 (1992) 259.
[22] S.H. Bauer, Chem. Rev. 96 (1996) 1907, and references therein.
[23] B.P. Lavrov, M. Osiac, A.V. Pipa, J. Ropcke, J. Plasma Sources Sci. Technol. 12 (2003) 576.
[24] M. Rayar, P. Veis, C. Foissac, P. Supiot, A. Gicquel, J. Phys. D Appl. Phys. 39 (2006) 2151.
[25] P.R. Rablen, J. Am. Chem. Soc. 119 (1997) 8350.
[26] C.-H. Chin, A.M. Mebel, D.-Y. Hwang, J. Phys. Chem. A 108 (2004) 473.
[27] R.P. Clarke, R.N. Pease, J. Am. Chem. Soc. 73 (1951) 2132.
[28] D.S. Dandy, M.E. Coltrin, J. Appl. Phys. 76 (1994) 3102.
[29] C. Wolden, K.K. Gleason, Appl. Phys. Lett. 62 (1993) 2329.
[30] L. Schafer, C.-P. Klages, U. Meier, K. Kohse-Hoinghaus, Appl. Phys. Lett. 58 (1991) 571.
[31] L.L. Connell, J.W. Fleming, H.-N. Chu, D.J. Vestyck Jr., J.E. Butler, J. Appl. Phys. 78 (1995) 3622.
[32] I. Langmuir, G.M.J. Mackay, J. Am. Chem. Soc. 36 (1914) 1708.
[33] S. Schwarz, S.M. Rosiwal, M. Frank, D. Breidt, R.F. Singer, Diamond Relat. Mater. 11 (2002) 589.
[34] B. Stefanov, L. Zarkova, J. Phys. D Appl. Phys. 9 (1976) 1217.
[35] D.W. Comerford, Ph.D. Thesis, University of Bristol, 2007.
[36] P.W. May, Yu.A. Mankelevich, J. Phys. Chem. C 112 (2008) 12432.
[37] P.W. May, J.N. Harvey, N.L. Allan, J.C. Richley, Yu.A. Mankelevich, J. Appl. Phys. 108 (2010) 014905.